

An Open Torque-Controlled Modular Robot Architecture for Legged Locomotion Research

Felix Grimmering*, Avadesh Meduri^{*,†}, Majid Khadiv*, Julian Viereck^{*,†}, Manuel Wüthrich*
 Maximilien Naveau*, Vincent Berenz*, Steve Heim**, Felix Widmaier*, Jonathan Fiene**
 Alexander Badri-Spröwitz** and Ludovic Righetti^{*,†}

Abstract—We present a new open-source torque-controlled legged robot system, with a low cost and low complexity actuator module at its core. It consists of a low-weight high torque brushless DC motor and a low gear ratio transmission suitable for impedance and force control. We also present a novel foot contact sensor suitable for legged locomotion with hard impacts. A 2.2 kg quadruped robot with a large range of motion is assembled from 8 identical actuator modules and 4 lower legs with foot contact sensors. To the best of our knowledge, it is the most lightest force-controlled quadruped robot. We leverage standard plastic 3D printing and off-the-shelf parts, resulting in light-weight and inexpensive robots, allowing for rapid distribution and duplication within the research community. In order to quantify the capabilities of our design, we systematically measure the achieved impedance at the foot in static and dynamic scenarios. We measured up to 10.8 dimensionless leg stiffness without active damping, which is comparable to the leg stiffness of a running human. Finally, in order to demonstrate the capabilities of our quadruped robot, we propose a novel controller which combines feedforward contact forces computed from a kino-dynamic optimizer with impedance control of the robot center of mass and base orientation. The controller is capable of regulating complex motions which are robust to environmental uncertainty.

I. INTRODUCTION

Present-day robot hardware is often mechanically complex and costly, different robot systems are hard to compare to each other, and legged robots are seldom commercially available. As a consequence, it is often difficult to test advanced control and learning algorithms without significant hardware development efforts or maintenance costs. To support rapid and broad progress in academic research, we believe a change in strategy is required. Hardware, firmware, and middle-ware must become inexpensive and easy to reproduce and implement. **Open-source blueprints of low-cost legged robot platforms** like [17], [31], and ours, will

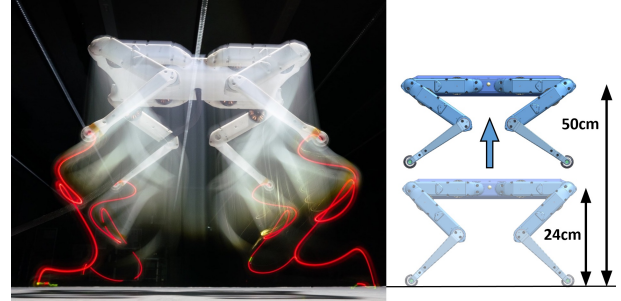


Fig. 1: Quadruped robot Solo performing a vertical 50 cm jump from its standing position. We assembled each leg from two identical brushless actuator modules, a lower leg segment, and a foot contact switch. (Picture by W. Scheible)

allow researchers to test and develop their ideas on a **wide variety of robotic platforms** with different morphologies. Performance and characteristics of legged robots reproduced from open-sourced blueprints can directly be compared with each other, anywhere in the world.

Open-source legged robotics can only become effective if little machining of parts is required to reproduce the blueprints, which is the endeavour of the presented work. This requirement excludes sophisticated actuator solutions with excessive, high-tolerance machining and it would be desirable to assemble the actuator modules from off-the-shelf parts only. To achieve this goal, we can benefit from inexpensive **plastic 3D printing** and high-performance brushless DC motors which became widely available lately, often as off-the-shelf hobbyist components. Furthermore, we can tap into the growing mobile device market for affordable sensors, low power and high-performance micro-controllers and increasing battery capacity.

Low-weight, inexpensive yet robust robots are particularly relevant when testing advanced algorithms for dynamic locomotion [4], [23], [24]. Indeed, simple robot operation and collaborative development through open-source initiatives can accelerate testing cycles. Low-weight robots require no cranes or complex guiding structures, can be operated by a single researcher and require less laboratory space. They can also significantly reduce the time and cost required for repair and maintenance. These features become especially important when testing learning algorithms directly on real hardware [33], [34] where it is essential to have a safe platform to explore various control patterns.

* Max Planck Institute for Intelligent Systems, 72076 Tübingen, Germany. Email first.lastname@tuebingen.mpg.de

** Max Planck Institute for Intelligent Systems, 70569 Stuttgart, Germany. Email lastname@is.mpg.de

† Tandon School of Engineering, New York University, Brooklyn, USA. Email first.lastname@nyu.edu

Part of this work was supported by the Max-Planck Society, New York University, the Max-Planck Institute for Intelligent Systems Grassroots projects, the European Unions Horizon 2020 research and innovation program (grant agreement 780684 and European Research Councils grant 637935), the National Science Foundation (CMMI-1825993) and a Google Faculty Research Award. We would like to thank Joel Bessekon Akpo for his help with the motor driver testing and Joshi Walzog for his help with the foot sensor circuit board layout.

Towards these goals, we present a novel, **fully open-source, modular force-controlled leg architecture** for dynamic legged robot research. This paper presents five main contributions: 1) a novel light-weight, low-complexity, torque-controlled actuator module suitable for impedance and force control, 2) a foot contact sensor suitable for legged robots withstanding hard impacts, 3) a complete characterization of the achieved impedance with one leg constructed with the actuator modules and foot sensor, demonstrating effective dimensionless impedance within the range of human running, 4) a 2.2 kg quadruped robot, Solo, assembled from 4 legs, with a very large range of motion and which is, to the best of our knowledge, the lightest force-controlled quadruped and 5) a torque-controller tracking full-body motions computed with a kino-dynamic motion optimizer [9], [24], demonstrating for the first time that motions computed with this motion optimizer can be executed on real robots under moderate environmental uncertainty. The complete design requires mostly 3D printed parts and off-the-shelf components, except for three small machined parts, and is fully open-sourced, including mechanical drawings, electronic circuits and control software [1].

II. RELATED WORK

Initial robot design choices often relate to form-factor and type of motor, its gear ratio, and gear type. Seok and colleagues [30] demonstrate that flat brushless direct current (BLDC) motors lead to high performance and low weight actuators ('high torque density'). With low gear ratio, often between 5:1 and 25:1, proprioceptive actuation can be achieved [5], [25], [30]. Proprioceptive actuators do not require dedicated force sensors as joint torque is directly estimated from motor phase current measurement [35].

Harmonic drive gear boxes are compact, relatively lightweight and have successfully been used for quadruped robot actuation [12], [21]. Unfortunately, their relatively high cost makes them unattractive for our project. Low-g geared actuators have the advantage of low friction and stage losses. Fewer and smaller parts in the gear train will induce lower losses from reflected inertia at oscillating load types [26]. 'Transparent' actuator concepts became standard in haptic devices for direct force feedback [8]. However, haptic devices require much lower output power compared to dynamic legged robot systems [35].

BLDC motors have higher output power to weight ratio, compared to previously used brushed motors. High power BLDC motors now offer the mechanically simpler solution to 'direct-drive' robot legs, without gearing [18]. With loads experienced by quadruped robots, calculations by [5], [26], [31] show that energy consumption can be reduced, and actuators used more efficiently with a low-g geared actuator.

Legged robots experience high peak torques from impacts, which can damage the gear train components. Hence, simple spur-gear trains with little contact surface between gears are rare in jumping robots or they are combined with mechanical compliance mounted in leg length- [22], [28] or leg-angle direction [6]. Planetary gears share loading among multiple

teeth [35]. Cable [14], [20], belt [25], and chain-driven [13], [16] actuators exhibit high robustness against external peak torque and can transmit power over a larger distance at low reflected inertia. Here, we use a low weight, dual-stage timing belt transmission with 9:1 gear reduction.

The Oncilla robot [31] and Stanford-doggo [17] are notable open-source robot platforms. Robots like Oncilla or Cheetah-cub [32] feature mechanical compliance in parallel to the leg actuation and react intrinsically and immediately to external perturbations [32]. However, these mechanisms would require complicated mechanisms to alter the joint stiffness effectively [11]. Stanford-doggo is torque controlled but, to the best of our knowledge, there is no report on the actual force control performance. These robots nevertheless require substantial machining, which is in contrast to our approach which require mostly off-the-shelf and 3D printed parts (except for the motor shaft and pulleys that need to be machines from stock material) and provides a torque-controlled platform which affords experimentation with state of the art controllers.

We designed our legged robot architecture for proprioceptive force-control. Such approaches require no additional sensing for locomotion on flat and level ground. But it becomes difficult in complex terrain to reliably estimate rapid, low-force contacts merely with proprioceptive control. Limited proprioceptive estimator accuracy has been compensated by appropriate filtering [3]. Here we chose to combine proprioceptive control with traditional, robust sensing by a distally mounted touch sensor. Only a few sensing principles remain functional at harsh impact conditions, like high-speed leg touchdowns. Peak forces can exceed two times bodyweight when exerted onto a single foot [35]. Light-weight force-sensing based on piezoresistive or optical sensing of deflecting elastic material has been demonstrated previously [19], [25]. Other designs measure the deflection of rubber-like materials through embedded magnets [2] or measure impacts with inertial measurement units [15]. These sensing concepts are relatively complex. Here we propose a simple and inexpensive design based on a spring-loaded aperture, similar to the principle implemented by Hsieh [10].

III. PLATFORM AND ROBOT OVERVIEW

This section details the actuator and contact sensor concepts for our modular leg design leading to a 2 DOF leg, and the quadruped robot Solo.

A. Actuator Concept

a) *Brushless Actuator Module:* The actuator module is shown in Figure 2a. It consists of a brushless motor (T-Motor Antigravity 4004, 300kV), a 9:1 dual-stage timing belt transmission (Conti Synchroflex AT3 GEN III), a high-resolution optical encoder (Avago AEDM 5810) and a 5000 cpr code wheel mounted directly on the motor shaft. Everything is contained inside the light-weight, 3D printed shell, with no exposed wires. The low transmission ratio enables reasonable peak torques and high velocity at the joint. Importantly, it ensures sufficient transparency to enable

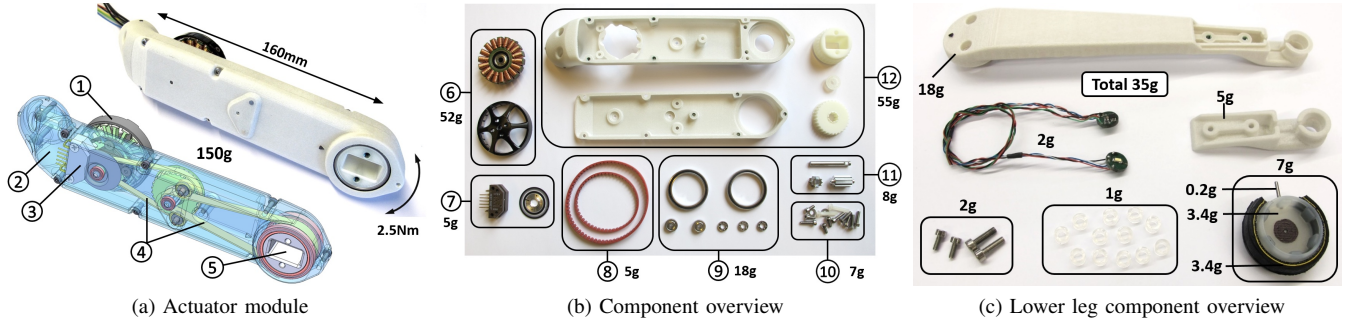


Fig. 2: Brushless actuator module (a) assembled, and (b) individual parts. BLDC motor ①, two-part 3D printed shell structure ②, high resolution encoder ③, timing belts ④, and output shaft ⑤. Brushless motor ⑥, optical encoder ⑦, timing belts ⑧, bearings ⑨, fasteners ⑩, machined parts ⑪ and 3D printed parts ⑫. With the exception of ⑪, all parts are either off-the-shelf, or printable on a regular 3D printer. The motor shaft and the pulleys ⑪ can be machined from stock material. (c) Lower leg and foot contact switch components.

accurate torque control through motor current measurements alone. The module weighs 150g for a segment length of 160mm and can output 2.5Nm joint torque at 12A. The assembly of the module is simple and requires very few components, as can be seen in Figure 2b. All components are either available off-the-shelf or can be 3D printed except for the motor shaft and the pulleys, which need to be machined from stock material.

b) Electronics: We initially purchased off-the-shelf TI micro-controller evaluation boards equipped with two BLDC booster cards each (Fig. 3b ⑬). This BLDC motor driver boards are capable of Field Oriented Control (FOC), and execute dual motor torque control at 10kHz (Fig. 3a). For a more compact design, we miniaturized the motor driver electronics, leading to a factor six reduction in weight, and a factor ten in volume reduction (Fig. 3b). The resulting MPI Micro-Driver electronics ⑭ consist of a Texas Instruments micro-controller (TMS320F28069M) and two motor driver chips (DRV8305) on a single board. The MPI Micro-Driver board is equipped with a CAN port for communication and a JTAG port for programming. Each BLDC motor driver board is supplied with 24V, by a dedicated power supply. Note that the TI micro-controller and our custom board provide the exact same functionality and can be used interchangeably, the custom electronics being smaller.

B. Foot Contact Sensor

The foot contact sensor (Figure 3c) was designed to withstand substantial impacts, for rapid contact detection at a low force threshold. Since the foot's point-of-contact is often unpredictable in rough terrain, we designed the switch to activate with a sensing range of 270° , which ensures proper contact detection for a wide range of robot configurations on complex terrains. We implemented a mechanism based on a light-emitting diode ⑮ and a light sensor ⑰. Both are separated by a spring-loaded, mechanical aperture ⑱ with 1.5mm diameter. The sensitivity of the contact switch can be adjusted by changing the diameter, length or number of elastic silicone elements utilized ⑲. External forces shift the aperture up to 2mm and generate an analog output signal

between 0V and 3V that is evaluated by an A/D converter on the micro-controller. The foot structure is 3D printed from plastic (Fig. 2c). It weighs 10g, triggers reliably at 3N within 2ms of contact. The sensor is simple to assemble, has high sensitivity and low response time while it can also withstand high impacts with the environment. This makes it suitable to detect contacts during dynamic locomotion tasks. It is mounted on the lower leg, which itself is a passive 3D printed structure.

C. 2-DOF Leg and Quadruped Robot Solo

A single, 2-DOF leg (Fig. 4a) is composed of two identical brushless actuator modules (hip ⑲, upper leg ⑳), and a passive lower leg ㉑. The foot ㉒ is mounted distally, at the end of the lower leg. All active joints are multi-turn capable. Cable routing between hollow segments limits rotations to about three turns in each direction.

We assembled the quadruped robot Solo from four identical legs and a 3D printed body structure (Figure 4c). The robot's eight DOF are mounted to enable movements in the sagittal plane. The trunk houses the motor driver electronics for controlling 8 BLDC motors. Solo is tethered for CAN bus communication and external power supply. The robot weighs 2.2kg, at about 0.24m standing hip height (maximum hip height of 0.34m), 0.42m body length, and 0.33m width. The robot can fold down to 5cm in height (Fig. 4c). It is also completely symmetric in all 3 axes of rotation.

D. Communication and Control Software

Both the 2-DOF leg and the quadruped are CAN bus tether connected, to an off-board PC running Ubuntu patched with RT-Preempt for real-time capabilities. The computer sends control commands for each individual leg and receives position and velocity sensor data from each joint at 1kHz. We implemented drivers to interface the electronics with the control PC. On the micro-controller, we use the TI-provided library for torque control and implemented custom software for sensor processing and communication over CAN. A C++ software package provides an API to interface with several motor boards from the PC, with basic functionalities for

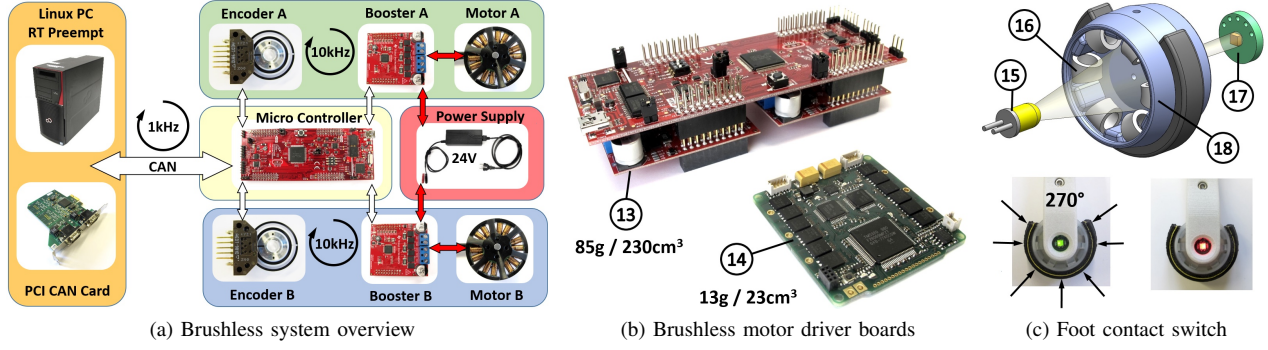


Fig. 3: **(a)** A CAN bus connects the PC to a micro controller board (TI evaluation board). Two brushless DC motors are controlled at 10 kHz from each node. High resolution encoders provide motor shaft position feedback. **(b)** We compacted an off-the-shelf TI Evaluation Board (13), into our MPI Micro-Driver electronics board (14). It controls two brushless motors, with feedback from two optical encoders. **(c)** Our custom foot contact switch, activating at a 270° wide range of impact directions, 2 ms after contact, and with a threshold of 3 N.

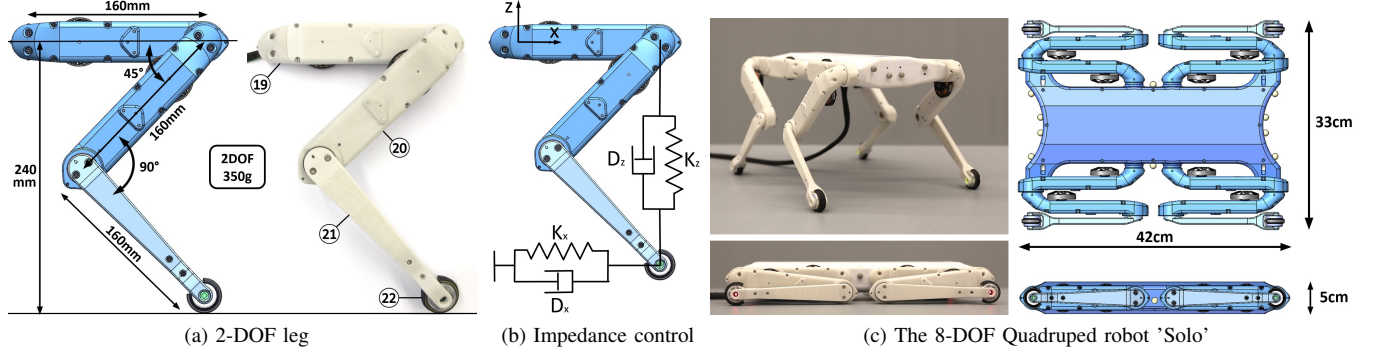


Fig. 4: **(a)** Assembly of two brushless actuator modules hip (19), and upper leg (20), lower leg (21), and foot contact switch (22). At 90° knee angle, the 2-DOF leg stands 0.24 m high, maximum hip height is 0.34 m. **(b)** Schematic presentation of impedance framework in Cartesian coordinates. **(c)** The 2.2 kg quadruped robot can fold into a 5 cm flat structure.

position and force control. The API also comes with Python bindings for rapid prototyping purposes. C++ functions enable the implementation of 1 kHz control loops necessary for force control. We provide several demo programs on the open-source repository [1], to e.g. rapidly test multi-actuator control.

IV. EXPERIMENTS AND RESULTS

In this section, we present experiments with the 2-DOF leg and the quadruped robot. First we quantify the impedance regulation properties of the system, then we present a controller to track motions optimized with a kino-dynamic optimizer and demonstrate dynamic behaviors on the quadruped robot.

A. Impedance control of the 2-DOF leg

We characterize the effective impedance control capabilities of the leg by measuring the range of stiffness that can be regulated in quasi-static and hard impact conditions. We built a test stand (Fig. 5) with instrumentation to characterize the leg's stiffness profile. We use a simple Cartesian impedance controller (Fig. 4b) to regulate the stiffness and damping of

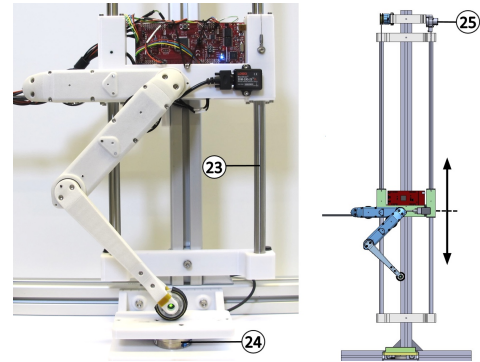


Fig. 5: Leg test stand with linear guide (23). A 6-axis ATI Mini40 force sensor (24) measured ground reaction forces. A string potentiometer measured leg height (25).

the foot with respect to the hip $\tau = J^T (K(x_d - x) - D\dot{x})$, where $x \in \mathbb{R}^2$ is the foot position with respect to the hip (leg length), $x_d \in \mathbb{R}^2$ the spring setpoint, J the foot Jacobian, K and D the desired leg stiffness and damping matrices and $\tau \in \mathbb{R}^2$ the vector of motor torques. Note that torque control is only based on the internal motor current and

motor position measurements without any force feedback. We validate the force control quality of the leg using external reference sensors on the test stand.

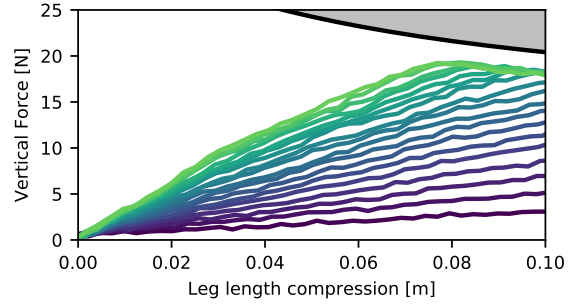
a) Quasi-static experiment: We systematically characterized the range of stiffnesses that can be regulated at the foot for quasi-static motions. The robot initially stands in a rest position, and we slowly pushed on the leg to produce a deflection. We measured the ground reaction force and the leg length using external ground-truth sensors (force plate and string potentiometer). In this experiment, $\mathbf{D} = \mathbf{0}$, and we only use the desired stiffness. We found we could regulate the range of desired stiffness between 20 N/m and 360 N/m, for slow motion. For larger stiffness, without damping, the leg would get unstable. Note that with small amounts of damping, the maximum stiffness can be increased further while avoiding unstable controller behavior (not shown here).

Results of the experiment are shown in Figure 6. We observe a close-to-linear relationship between vertical ground reaction force and vertical leg displacement for all desired stiffness values until the controller reaches actuator limits (Fig. 6a). The maximum leg force (black line) is limited due to a combination of actuator torque limit (maximum applied current), and leg kinematics. The linear relationship is independent of leg compression, suggesting that the linear impedance law works for a broad range of displacements (up to 10 cm for cases below torque saturation limits).

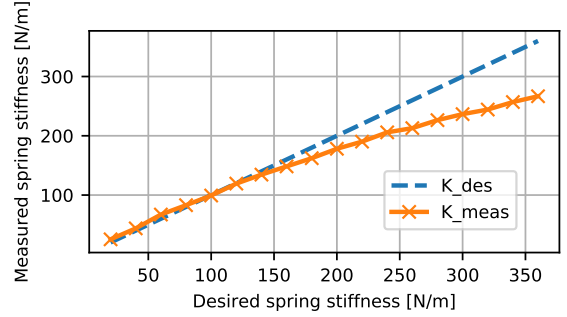
We computed the effective leg stiffness using linear regression, where we excluded data points in the saturation region. For commanded stiffness lower than 150 N/m, the measured leg stiffness matches the desired stiffness very well. At higher stiffness, we observe lower measured stiffness. Without damping, the maximum measured stiffness was ≈ 266 N/m for a commanded stiffness of 360 N/m. Note that the identification presented in Figure 6b could also help choose a command that will realize a reference stiffness.

These experiments demonstrate the ability of the robot to regulate leg stiffness with a simple control law and without the need for torque sensing. Experimental data shows the linearity of the force-displacement relationship. The difference in high stiffness regimes between actual and commanded stiffness is likely due to other dynamic effects including friction, the flexibility of the transmission and error in joint position measurements (i.e., the encoders measure motor displacement, not joint motion).

b) Drop experiment: The 2-DOF leg was dropped from a height of 0.24 m, with a desired leg stiffness of 150 N/m and low damping of 0.5 Ns/m. This experiment shows the leg's impedance capabilities: producing simultaneous high torques and speeds. Fig. 7 (top) shows the time evolution of the contact force for a typical drop test. The impact response of unsprung mass is visible as large, oscillating forces, during the first 50 ms of the impact. Frictional and deformation losses are visible by deviations from the ideal leg force: higher forces between touch-down and mid-stance, and lower forces between mid-stance and toe-off. Losses lead to a lower second peak amplitude, of 8 N. Leg forces settle at the system's weight of 6 N (weight of 2-DOF leg, vertical



(a) Force-displacement relationship



(b) Measured vs. desired stiffness

Fig. 6: Quasi-static experiment: **(a)** Vertical ground reaction force versus leg compression, for desired stiffness ranging from 20 N/m (purple line) to 360 N/m (green line) in 20 N/m increments. The black asymptotically falling curve indicates the theoretical maximum leg force, calculated from the maximum knee torque and two-segment leg kinematics. **(b)** Desired leg spring stiffness vs measured leg spring stiffness (slope from linear regression of the data shown in **(a)**).

slider, and electronics).

Fig. 7 (bottom) shows hysteresis in the work space, and indicates friction and losses in structural system deformation. The hysteresis can be explained by Coulomb friction shifting forces above and below the desired force, depending on the desired direction of motion. Hysteresis losses can be compensated with active control, however this was not the goal in this experiment. The low variance after impact shows very good repeatability of the system. The linear relationship between leg compression and ground reaction forces remained.

c) Jumping experiments: We have already demonstrated the jumping capabilities of a preliminary version of the leg in [34]. Here we implement a simple periodic vertical motion using joint position controllers to generate jumping behavior. The leg is capable of jumping approximately 0.65 m, which is roughly twice its leg length and 2.7 times its resting leg length. The robot lands without damage. This demonstrates the ability of our system to generate dynamic motions with force-control.

B. Dynamic behavior of the quadruped robot

In these experiments, we demonstrate the dexterity and capabilities of the quadruped robot. Moreover, we present

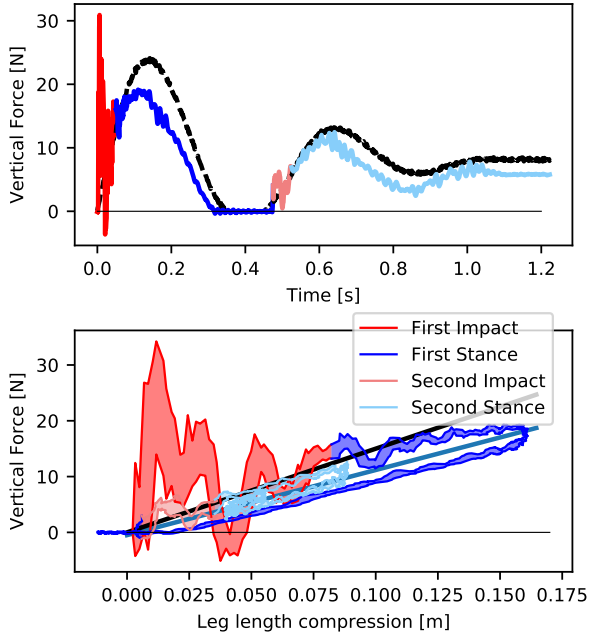


Fig. 7: 0.24 m drop experiments repeated ten times, with desired leg stiffness $k = 150$ N/m. The 2-DOF leg bounces twice. The first bounce is plotted in red and blue, the second bounce in light red and light blue. Desired stiffness is indicated with black lines. Top: leg force as a function of time for one typical experiment. Bottom: leg force as a function of leg compression, all ten experiments are summarized as an envelop defined by the average \pm the standard deviation. The blue straight line is the regressed approximation of the stance data ($K = 116$ and $D = 0.5$).

the first real robot experiments using motions computed with a centroidal dynamics-based kino-dynamic planner [9], [24].

a) Kino-dynamic motion optimizer and controller: The motions are planned using the full body kino-dynamic optimizer proposed in [9]. The algorithm alternatively optimizes 1) the centroidal dynamics of the robot (i.e. its center of mass, linear and angular momentum) together with contact forces trajectories and 2) the kinematics of the full body. After several iterations, a consensus between both optimization problems is reached, leading to locally optimal trajectories consistent with the full robot dynamics. In our experiments, consensus was typically achieved after two iterations. The centroidal dynamics optimization problem is solved using the algorithm proposed in [24].

Our control strategy consists in computing contact forces for the feet in contact such that they generate a sufficient wrench at the CoM to regulate reference CoM, angular momentum and base orientation trajectories. A low impedance controller for the motion of each foot is then added. First an overall desired wrench \mathbf{W}_{CoM} at the CoM is computed as

$$\mathbf{W}_{CoM} = \mathbf{W}_{CoM}^{ref} + \begin{bmatrix} \mathbf{K}_c(\mathbf{x}_c^{ref} - \mathbf{x}_c) + \mathbf{D}_c(\dot{\mathbf{x}}_c^{ref} - \dot{\mathbf{x}}_c) \\ \mathbf{K}_b(\mathbf{q}_b^{ref} \boxminus \mathbf{q}_b) + \mathbf{D}_b(\mathbf{k}^{ref} - \mathbf{k}) \end{bmatrix}$$

where \mathbf{x}_c , \mathbf{k} and \mathbf{q}_b are the measured CoM position, angular

momentum and base orientation (quaternion) respectively. ref denotes the reference trajectories from the motion optimizer, in particular \mathbf{W}_{CoM}^{ref} is the reference wrench at the CoM. \mathbf{K}_c , \mathbf{K}_b , \mathbf{D}_c and \mathbf{D}_b are gain matrices. The operator \boxminus is the operator that maps the rotation needed to correct for the orientation error between two quaternions into an angular velocity vector using the logarithm mapping between a Lie group and its Lie algebra. In this formulation, we assume that the CoM is located at the base frame origin (its location being therefore constant in this frame), which is a good approximation given that most of the robot mass is located in its base. We also assume that the locked inertia tensor is constant so we can mix orientation and angular momentum control meaningfully. These assumptions proved sufficient for good feedback control performance.

The force allocation for each foot in contact is then computed at each instant of time by solving the following simple quadratic program

$$\begin{aligned} \min_{\mathbf{F}_i, \eta} \quad & \sum_i \mathbf{F}_i^2 + \alpha(\eta^2 + \zeta_1^2 + \zeta_2^2) \\ \text{s.t.} \quad & \mathbf{W}_{CoM} = \sum_{i \in \mathcal{C}} \begin{pmatrix} \mathbf{F}_i \\ \mathbf{r}_i \times \mathbf{F}_i \end{pmatrix} + \eta \\ & F_{i,x} < \mu F_{i,z} + \zeta_1, \quad F_{i,y} < \mu F_{i,z} + \zeta_2 \quad \forall i \in \mathcal{C} \end{aligned}$$

where \mathcal{C} contains the indexes of the feet in contact with the ground (we tested the contact activation based on both the plan and the contact sensors feedback), η , ζ_1 and ζ_2 are slack variables that ensure that the QP has always a feasible solution, α is a large weight, \mathbf{r}_i is the vector from foot i to CoM, μ is the friction coefficient and z is the direction orthogonal to the ground. Once an optimal foot force allocation is found, the actuation torques are computed as

$$\boldsymbol{\tau}_i = \mathbf{J}_{i,a}^T \left(\mathbf{F}_i + \mathbf{K}(\mathbf{l}_i^{ref} - \mathbf{l}_i) + \mathbf{D}(\dot{\mathbf{l}}_i^{ref} - \dot{\mathbf{l}}_i) \right)$$

where $\mathbf{J}_{i,a}$ is the actuated part of the foot Jacobian, \mathbf{l} is the vector between the foot and the base origin and the index i corresponds to each leg.

b) Solo motion capabilities: Solo's leg joints are multi-turn capable, up to three turns in each direction. Figure 8 illustrates how Solo can exploit these capabilities in various situations. Solo's knee joints can be bent in both directions, and configure the robot into 'X', 'O'-knee postures, or forward- and backward 'C' postures when required (Fig. 8a). It bends its knee joint backward, to reach the obstacle from the top (Fig. 8b). We designed a simple motion sequence (Fig. 8c), allowing Solo to stand up after a turn-over. We note that the three demonstrated behaviors cannot be kinematically achieved by quadruped animals.

c) Tracking kino-dynamic plans: We first test the controller in different balancing scenarios that can be seen in the accompanying video. The results show that the robot is capable of balancing on moving platforms without any knowledge of the environment. Then we compute a jumping motion, a slow and a fast walk. Results show that the robot can follow the desired plans. It is interesting to note that

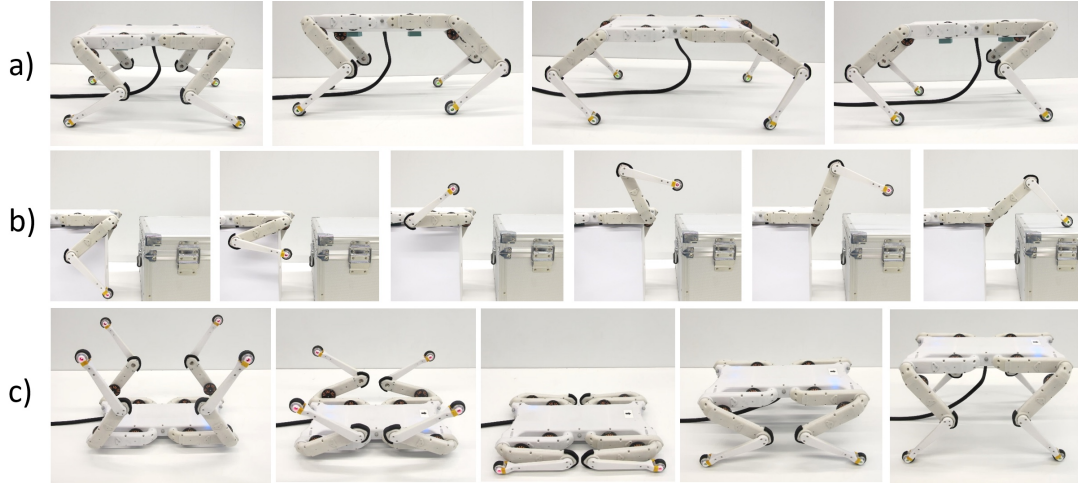


Fig. 8: Example motion sequences: a) Legs can switch between all the four knee configurations, b) with more than 360° hip joint rotation capability, and little space to navigate, legs can be rotated first backwards, and then onto a step, c) in case the robot falls onto its back, it can re-orient its legs, and stand up without rotating the trunk.

the plans are rather long and that no re-planning is done in these experiments. Nevertheless, the robot is able to achieve the task. During the slow walk motion, we added a seesaw obstacle that is not taken into account in the planner nor the controller. The robot is able to traverse the terrain without any problems. These results suggest that the controller is robust to the uncertain environments and can adequately stabilize long motion plans. Moreover, this demonstrates that the plans generated by the kino-dynamic optimizer can be transferred to a real robot despite the difference between the dynamic model of the robot and the real system and that they are robust to moderate disturbances. The accompanying video demonstrates all these behaviors. The robot was able to jump vertically, its base reaching 0.53 m with respect to the ground (Fig. 1), and land without damage.

V. DISCUSSION

a) Design choices: Designing a low-weight quadruped robot, while maintaining effective impedance and force control capabilities required us to trade-off several design features. We mounted lower-cost hobbyist BLDC motors. These motors exhibit torque ripples at very low speed, which so far was not a problem during normal locomotion operation but might necessitate active compensation for certain slow precision tasks. We measure torque at the motor, through current measurement. For this, we directly use the data provided by the BLDC motor driver boards. The resulting output torque at the end effector differs due to gear losses, belt and leg structural flexibility, and inertial losses. Nevertheless, our experimental results show that very good impedance control is possible. The robot’s leg joints have multi-turn capability which allows the quadruped robot to switch between four knee configurations, and directly re-orient itself after falling on its back. The large range of motion simplifies motion planning when faced with obstacles along the path.

We have demonstrated legs assembled from the same actuator module but other configurations are also possible. Multiple legs modules can be used as manipulators when reconfigured into a large hand-like structure. We are also currently designing a 12-DOF quadruped with adduction/abduction degree of freedom at the hip joint. We also plan to replace current CAN-based wired communication with wireless, and add on-board battery power for full mobility.

b) Impedance control capabilities: The systematic characterization of leg stiffness suggests that the actuator module can serve as a basis to construct high performance force-controlled robots. As a comparison, reported human leg stiffness values at running [7] ranges from $k = 7 \text{ kN/m}$ to 16.3 kN/m . For a 75 kg, 1 m leg length human, this translates into a dimensionless leg stiffness, $\tilde{k} = k \cdot l_0 / (mg)$ [27], between $\tilde{k} = 10$ and 22. In our 2-DOF leg experiments we measured 266 N/m stiffness, corresponding to dimensionless leg stiffness of 10.8, putting the capabilities of the robot within a range comparable to human leg stiffness. Comparison with other quadruped robots is difficult as impedance or force control performance is seldom characterised. Semini and colleagues characterized the 10 kg, hydraulically driven HyQ leg and from their reported results [29, Fig 12] we estimate a dimensionless HyQ leg stiffness of $\tilde{k} = 5250 \text{ N/m} \cdot 0.3 \text{ m} / (10 \text{ kg} \cdot 9.81 \text{ m/s}^2) = 16$, which is slightly higher than the leg’s dimensionless stiffness of our quadruped.

c) Open Source and Outreach: Mechanical and electrical hardware blueprints and software required for this project are open-source under the BSD-3-clause license. All the sources are available at [1] and the robots can be easily reproduced and improved by other laboratories. At the moment, 3 other laboratories are in the process of producing their own copy of the quadruped. The actuator module is inexpensive, and the full quadruped was built for approximately 4000€ of material cost. The low weight and simplicity of the robot allow for easy transportation and safe operation, significantly

simplifying experimental environments. The platform can also be used as an educational tool. We use the leg, for example, to teach robotics to high school interns at New York University.

VI. CONCLUSION AND FUTURE WORK

We presented an open-source low-cost actuator module and a foot contact sensor used to build torque-controlled legged robots. We developed the system's hardware, electronics, and firmware/software to support legged robot locomotion research with a rugged and durable, low-weight robot that can be handled safely by a single researcher. Experiments show the capabilities of the robots in generating very dynamic motions with excellent impedance regulation characteristics. In particular, we introduced a simple torque-controller capable of regulating motions generated with a state of the art kino-dynamic optimizer. We anticipate that the open-source aspect of the project will further benefit the robotics community by lowering the barrier to entry and lead to fruitful extensions of the robots.

REFERENCES

- [1] "Open dynamic robot initiative," <https://open-dynamic-robot-initiative.github.io/>.
- [2] A. Ananthanarayanan, S. Foong, and S. Kim, "A compact two dof magneto-elastomeric force sensor for a running quadruped," in *IEEE Int. Conference on Robotics and Automation*, 2012, pp. 1398–1403.
- [3] G. Bledt, P. M. Wensing, S. Ingersoll, and S. Kim, "Contact model fusion for event-based locomotion in unstructured terrains," in *IEEE Int. Conference on Robotics and Automation*, 2018, pp. 1–8.
- [4] J. Carpentier and N. Mansard, "Multicontact locomotion of legged robots," *IEEE Trans. on Robotics*, vol. 34, no. 6, pp. 1441–1460, 2018.
- [5] Y. Ding and H.-W. Park, "Design and Experimental Implementation of a Quasi-Direct-Drive Leg for Optimized Jumping," in *IEEE/RSJ Int. Conference on Intelligent Robots and Systems*, 2017, pp. 300–305.
- [6] P. Eckert, A. E. Schmerbach, T. Horvat, K. Söhnle, M. S. Fischer, H. Witte, and A. J. Ijspeert, "Towards rich motion skills with the lightweight quadruped robot Serval," *Adaptive Behavior*, p. 1059712319853227, 2019.
- [7] C. T. Farley and O. Gonzalez, "Leg stiffness and stride frequency in human running," *J. of Biomechanics*, vol. 29, no. 2, pp. 181–186, 1996.
- [8] D. V. Gealy, S. McKinley, B. Yi, P. Wu, P. R. Downey, G. Balke, A. Zhao, M. Guo, R. Thomasson, A. Sinclair *et al.*, "Quasi-direct drive for low-cost compliant robotic manipulation," *arXiv preprint arXiv:1904.03815*, 2019.
- [9] A. Herzog, S. Schaal, and L. Righetti, "Structured contact force optimization for kino-dynamic motion generation," in *IEEE/RSJ Int. Conference on Intelligent Robots and Systems*, 2016, pp. 2703–2710.
- [10] S. T. Hsieh, "Three-axis optical force plate for studies in small animal locomotor mechanics," *Review of Scientific Instruments*, vol. 77, no. 5, p. 054303, May 2006.
- [11] J. W. Hurst and A. A. Rizzi, "Physically variable compliance in running," in *Climbing and Walking Robots*. Springer, 2005, pp. 123–133.
- [12] M. Hutter, C. Gehring, D. Jud, A. Lauber, C. D. Bellicoso, V. Tsounis, J. Hwangbo, K. Bodie, P. Fankhauser, M. Bloesch *et al.*, "Anymal-a highly mobile and dynamic quadrupedal robot," in *IEEE/RSJ Int. Conference on Intelligent Robots and Systems*, 2016, pp. 38–44.
- [13] M. Hutter, C. D. Remy, M. A. Hoepflinger, and R. Siegwart, "Scarleth: Design and control of a planar running robot," in *IEEE/RSJ Int. Conference on Intelligent Robots and Systems*, 2011, pp. 562–567.
- [14] J. Hwangbo, V. Tsounis, H. Kolvenbach, and M. Hutter, "Cable-driven actuation for highly dynamic robotic systems," in *IEEE/RSJ Int. Conference on Intelligent Robots and Systems*, 2018, pp. 8543–8550.
- [15] R. Käslin, H. Kolvenbach, L. Paez, K. Lika, and M. Hutter, "Towards a passive adaptive planar foot with ground orientation and contact force sensing for legged robots," in *IEEE/RSJ Int. Conference on Intelligent Robots and Systems*, 2018, pp. 2707–2714.
- [16] B. Katz, J. Di Carlo, and S. Kim, "Mini cheetah: A platform for pushing the limits of dynamic quadruped control," in *IEEE-RAS Int. Conference on Robotics and Automation*, 2019, pp. 6295–6301.
- [17] N. Kau, A. Schultz, N. Ferrante, and P. Slade, "Stanford doggo: An open-source, quasi-direct-drive quadruped," *arXiv preprint arXiv:1905.04254*, 2019.
- [18] G. Kenneally, A. De, and D. E. Koditschek, "Design principles for a family of direct-drive legged robots," *IEEE Robotics and Automation Letters*, vol. 1, no. 2, pp. 900–907, 2016.
- [19] J.-C. Kim, K.-S. Kim, and S. Kim, "Note: A compact three-axis optical force/torque sensor using photo-interrupters," *Review of Scientific Instruments*, vol. 84, no. 12, p. 126109, 2013.
- [20] S. Kitano, S. Hirose, A. Horigome, and G. Endo, "TITAN-XIII: sprawling-type quadruped robot with ability of fast and energy-efficient walking," *ROBOMECH Journal*, vol. 3, no. 1, pp. 1–16, Mar. 2016.
- [21] Y. H. Lee, Y. H. Lee, H. Lee, L. T. Phan, H. Kang, Y. B. Kim, and H. R. Choi, "Development of torque controllable leg for running robot, aidin-iv," in *IEEE/RSJ Int. Conference on Intelligent Robots and Systems*, 2017, pp. 4125–4130.
- [22] F. Meyer, A. Spröwitz, and L. Berthouze, "Passive compliance for a RC servo-controlled bouncing robot," *Advanced Robotics*, vol. 20, no. 8, pp. 953–961, 2006.
- [23] I. Mordatch, E. Todorov, and Z. Popović, "Discovery of complex behaviors through contact-invariant optimization," *ACM Trans. on Graphics (TOG)*, vol. 31, no. 4, p. 43, 2012.
- [24] B. Ponton, A. Herzog, A. Del Prete, S. Schaal, and L. Righetti, "On time optimization of centroidal momentum dynamics," in *IEEE Int. Conference on Robotics and Automation*, 2018, pp. 1–7.
- [25] J. Ramos and S. Kim, "Facilitating Model-Based Control through Software-Hardware Co-Design," in *IEEE Int. Conference on Robotics and Automation*, 2018.
- [26] F. Roos, H. Johansson, and J. Wikander, "Optimal selection of motor and gearhead in mechatronic applications," *Mechatronics*, vol. 16, no. 1, pp. 63–72, 2006.
- [27] J. Rummel and A. Seyfarth, "Stable Running with Segmented Legs," *Int. J. of Robotics Research*, vol. 27, no. 8, pp. 919–934, Aug. 2008.
- [28] R. Sato, I. Miyamoto, K. Sato, A. Ming, and M. Shimojo, "Development of robot legs inspired by bi-articular muscle-tendon complex of cats," in *IEEE/RSJ Int. Conference on Intelligent Robots and Systems*, 2015, pp. 1552–1557.
- [29] C. Semini, V. Barasuol, T. Boaventura, M. Frigerio, M. Focchi, D. G. Caldwell, and J. Buchli, "Towards versatile legged robots through active impedance control," *Int. J. of Robotics Research*, p. 0278364915578839, May 2015.
- [30] S. Seok, A. Wang, D. Otten, and S. Kim, "Actuator design for high force proprioceptive control in fast legged locomotion," in *IEEE/RSJ Int. Conference on Intelligent Robots and Systems*, 2012, pp. 1970–1975.
- [31] A. Spröwitz, A. Tuleu, M. Ajallooeian, M. Vespignani, R. Möckel, P. Eckert, M. DHaene, J. Degraeve, A. Nordmann, B. Schrauwen, J. Steil, and A. J. Ijspeert, "Oncilla Robot: A Versatile Open-Source Quadruped Research Robot With Compliant Pantograph Legs," *Frontiers in Robotics and AI*, vol. 5, 2018.
- [32] A. Spröwitz, A. Tuleu, M. Vespignani, M. Ajallooeian, E. Badri, and A. Ijspeert, "Towards Dynamic Trot Gait Locomotion: Design, Control and Experiments with Cheetah-cub, a Compliant Quadruped Robot," *Int. J. of Robotics Research*, vol. 32, no. 8, pp. 932–950, 2013.
- [33] J. Tan, T. Zhang, E. Coumans, A. Iscen, Y. Bai, D. Hafner, S. Bohez, and V. Vanhoucke, "Sim-to-real: Learning agile locomotion for quadruped robots," in *Proceedings of Robotics: Science and Systems*, 2018.
- [34] J. Viereck, J. Kozolinsky, A. Herzog, and L. Righetti, "Learning a structured neural network policy for a hopping task," *IEEE Robotics and Automation Letters*, vol. 3, no. 4, pp. 4092–4099, 2018.
- [35] P. M. Wensing, A. Wang, S. Seok, D. Otten, J. Lang, and S. Kim, "Proprioceptive Actuator Design in the MIT Cheetah: Impact Mitigation and High-Bandwidth Physical Interaction for Dynamic Legged Robots," *IEEE Trans. on Robotics*, vol. 33, no. 99, pp. 1–14, 2017.